




## OPTICALLY ACTIVE TiO<sub>2</sub> FILMS FABRICATED BY SPIN COATING METHOD FOR METHYLENE BLUE PHOTOREMEDIATION

Vicran Zharvan<sup>1</sup>, Gatut Yudhoyono<sup>2</sup>, Darminto<sup>2</sup>

<sup>1</sup>Laboratory of Materials Physics, Department of Physics,  
Universitas Negeri Makassar, Indonesia,  
e-mail: vicran.zharvan@unm.ac.id

<sup>2</sup>Department of Physics,  
Institut Teknologi Sepuluh Nopember, Indonesia

(Received 05 July 2023; in final form 16 January 2024; accepted 31 January 2024; published online 26 March 2024)

The spin-coating process was used to create the TiO<sub>2</sub> layer successfully. The TiO<sub>2</sub> film was created by dissolving TiO<sub>2</sub> nanopowder in terpineol and ethylcellulose, and then spin coating it onto the corning glass. The films' shape, phase, and optical properties were then determined using SEM, XRD, and UV-Vis. Photocatalytic measurements of TiO<sub>2</sub> films were performed using a UV lamp to irradiate a 12 mg/l methylene blue solution for 5 hours. According to the results, all TiO<sub>2</sub> films feature an anatase phase with crystallite size values ranging from 5.55 nm to 6.94 nm and an absorbance region near the UV range. The best photocatalytic activity was found in a film containing TiO<sub>2</sub> particles that had been stirred for 5 hours with the value of constant rate of discoloration dye 0.0032/min.

**Key words:** TiO<sub>2</sub>, anatase, thin-film, photocatalyst.

DOI: <https://doi.org/10.30970/jps.28.1801>

### I. INTRODUCTION

Titanium dioxide crystal formations include anatase, rutile, and brookite. Anatase, with a band gap of 3.20 eV, offers better photocatalytic capabilities than rutile or brookite [1]. As a result, when producing TiO<sub>2</sub> powder to be used as a photocatalyst, it is critical to pay close attention to factors such as crystal structure, morphology, and phase stability [2].

TiO<sub>2</sub> powders can be synthesized using various processes, such as chemical vapour deposition, hydrothermal method, and sol-gel method [3]. The TiO<sub>2</sub> powder of anatase modification with a crystallite size of 7 nm was produced by the sol-gel method [4]. Nano powder TiO<sub>2</sub> can also be synthesized by combustion, gas phase [2] or co-precipitation method [5]. The advantage of adopting the co-precipitation approach is that TiO<sub>2</sub> can be produced at low temperatures, and the particle size can be readily controlled. This method is expected to result in smaller particle sizes and more homogeneous and bigger sizes than the sol-gel method [6]. One of the parameters can be varied by varying the mixing time [7]. A previous study [8] found that the TiO<sub>2</sub> nanopowders synthesized by varying the mixing duration at 5 h, 10 h, and 25 h have an anatase phase with crystallite size values of 11.83 nm, 10.7 nm, and 9.6 nm for time durations of 5, 10, and 25 h, respectively.

TiO<sub>2</sub> can purify the environment and dissolve dye in its application [9]. Making a thin TiO<sub>2</sub> film is one way to accomplish this. Semiconducting TiO<sub>2</sub> films can be obtained by dip coating, sputtering, CVD, MCCVD, and the spin coating methods [10–12]. The fabrication of a TiO<sub>2</sub> thin film has been extensively researched. Authors effectively manufactured a TiO<sub>2</sub> thin film with an anatase phase and grain size of 19 nm [13], and other researchers produced a thin film of TiO<sub>2</sub> with a band gap energy between 3.4 eV to 3.7 eV [14, 15].

In the present study, optically active films of TiO<sub>2</sub> with crystallite size of 5.55–6.94 nm were synthesized by the spin-coating method for the photocatalytic remediation of methylene blue (MB) as a model pollutant.

### II. EXPERIMENTAL METHOD

TiO<sub>2</sub> films were first created by dissolving the time-varying TiO<sub>2</sub> powder [8] in terpineol and ethylcellulose in a 1:1:1 weight ratio of TiO<sub>2</sub> powder, terpineol and ethylcellulose. These organic substances are employed as binders to enhance the viscosity of the TiO<sub>2</sub> dispersion solution and to produce a porous TiO<sub>2</sub> layer after undergoing the sintering process [16]. The solution was sprayed onto a glass substrate cleaned with ethanol and deionized water. The substrate was placed on the spin coater with a TiO<sub>2</sub> solution and rotated at 3500 rpm for 120 seconds. After 15 minutes of heating at 400°C, film coatings of TiO<sub>2</sub> were produced. The films were then analyzed using X-ray diffraction (Xpert MPD), scanning electron microscopy (SEM) (VEGA3 TESCAN), and a UV-Vis spectrophotometer (GENESYS 10S UV-Vis) to determine their crystal structure and optical properties.

The photocatalytic activity of TiO<sub>2</sub> films was determined by degrading 12 ppm of methylene blue under UV irradiation. The TiO<sub>2</sub> film was settled in a glass containing 20 ml methylene blue solution. The solution was then stirred for 15 minutes in the dark condition to achieve an equilibrium of absorption/desorption on the film photocatalyst. The solution and the film were exposed to UV irradiation (25 W) for 5 h. The solution was then analyzed using a UV-Vis spectrophotometer (GENESYS 10S UV-Vis) to obtain an absorbance value at 665 nm wavelength.



Sample	Mass of substrate before coating (g)	Mass of substrate after coating (g)	Mass of TiO <sub>2</sub> (mg)	Crystallite size (nm)
TiO <sub>2</sub> – 5 h	1.6878	1.6890	1.2	5.55
TiO <sub>2</sub> – 10 h	1.3808	1.3813	0.5	7.66
TiO <sub>2</sub> – 25 h	1.4970	1.4975	0.5	5.94
TiO <sub>2</sub> – 5 h (3x coatings)	1.4644	1.4669	2.5	6.54
TiO <sub>2</sub> – 5 h (5x coatings)	1.3770	1.3870	10	6.94
Commercially TiO <sub>2</sub>	1.4832	1.4833	0.1	

Table 1. Structure of TiO<sub>2</sub> films

Sample	<i>a</i> (nm)	<i>b</i> (nm)	<i>c</i> (nm)	<i>c/a</i>	<i>d</i> <sub>101</sub> (nm)	χ <sup>2</sup>
TiO <sub>2</sub> – 5 h	3.808502	3.808502	9.231786	2.423994	0.352067	1.04
TiO <sub>2</sub> – 10 h	3.875504	3.875504	8.366173	2.158732	0.351653	1.00
TiO <sub>2</sub> – 25 h	3.887733	3.887733	9.609140	2.471656	0.360394	3.33
TiO <sub>2</sub> – 5 h (3x coatings)	3.787205	3.787205	9.477464	2.502496	0.351682	2.73
TiO <sub>2</sub> – 5 h (5x coatings)	3.786964	3.786964	9.475038	2.502014	0.351650	2.97
TiO <sub>2</sub>	3.789	3.789	9.493	2.50541	0.351905	1.79

Table 2. Rietveld refinement results of TiO<sub>2</sub> films fabricated by the spin coating method

### III. RESULTS AND DISCUSSION

#### A. X-ray diffraction

Figure 1 shows the X-ray diffraction pattern of TiO<sub>2</sub> films fabricated by the spin coating method. Based on Fig. 1, it was evident that each of the sample TiO<sub>2</sub> films has a peak at  $2\theta = 25.3^\circ$  (011), which is an anatase phase, suggesting that there is no change in phase and that the properties are the same as those of TiO<sub>2</sub> that has been synthesized [8]. However, there is a difference in intensity. The film that uses commercial (Degussa P25) TiO<sub>2</sub> powder has the highest intensity compared to the other samples. It shows that the film that uses TiO<sub>2</sub> commercial has good crystallinity. Besides, films using synthesized TiO<sub>2</sub> powder are amorphous and show broad anatase phase peaks, suggesting the small crystallite size existing in that sample [17] or semicrystallite forms [18].

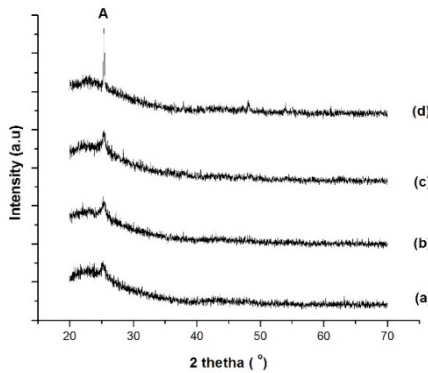


Fig. 1. XRD pattern of TiO<sub>2</sub> films: a) TiO<sub>2</sub> – 5 h, b) TiO<sub>2</sub> – 10 h, c) TiO<sub>2</sub> – 25 h, and d) commercial TiO<sub>2</sub> powder (A = anatase)

Figure 2 shows the X-ray diffraction pattern of TiO<sub>2</sub> – 5 h films by varying the number of coatings (1, 3 and 5 times coatings). As shown in Fig. 2, the intensity of diffraction at  $2\theta = 25.3^\circ$  (011) increases with an increase in the number of coatings due to an increase in the amount of TiO<sub>2</sub> powder on the substrate. It shows that the sample with five times coatings has the largest crystallite size [18]. Consequently, the intensities of other peaks at  $2\theta = 25.3^\circ$  (011),  $37.8^\circ$  (101),  $48.1^\circ$  (012),  $53.9^\circ$  (110), and  $62.8^\circ$  (111) of the anatase phase were increased and gave information that the sample TiO<sub>2</sub> – 5 h film with five times of coating has a good crystallinity [19, 20]. Table 1 shows the crystallite size determined using the Debye–Scherrer equation [21] and the mass of the catalyst of TiO<sub>2</sub> films fabricated by the spin coating method as a variation of time mixing duration and some coatings. It can be seen that increasing the number of coatings will increase the crystallite size value due to the increase in the catalyst mass causing more grain and aggregates [22].

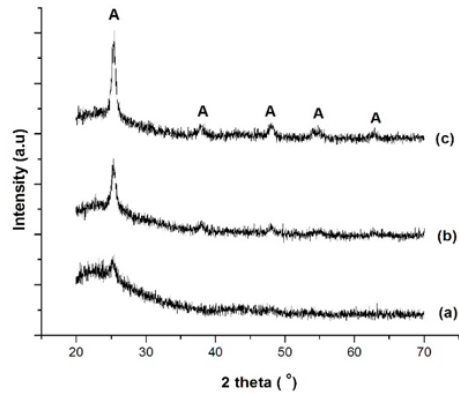


Fig. 2. XRD patterns of TiO<sub>2</sub> – 5 h films with varying number of coatings: a) 1x, b) 3x, and c) 5x (A = anatase)

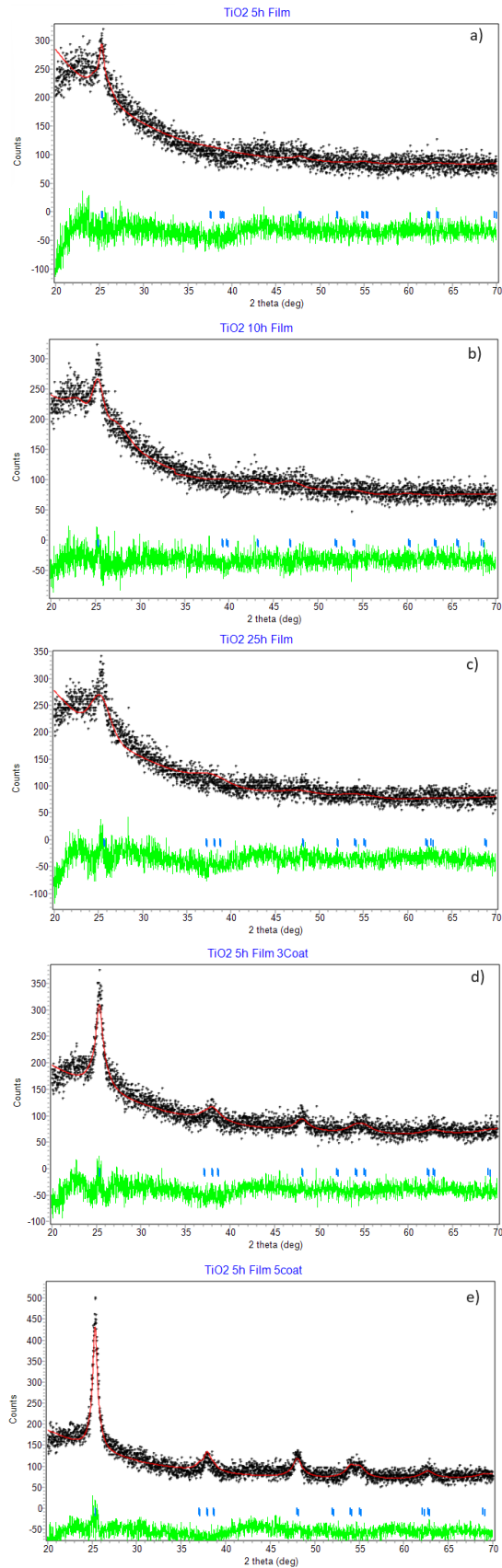


Fig. 3. Rietveld refinement pattern of a)  $\text{TiO}_2$  – 5 h, b)  $\text{TiO}_2$  – 10 h, c)  $\text{TiO}_2$  – 25 h, d)  $\text{TiO}_2$  – 5 h (3x coatings), and e)  $\text{TiO}_2$  – 5 h (5x coatings)

Further analysis of the crystal structure to determine lattice parameters can be carried out using the Rietveld refinement method with the application of Rietica software. The refinement results indicate that all  $\text{TiO}_2$  films exhibit a tetragonal crystal structure with the space group I 41/a m d. This result aligns with those obtained by Preeti and Sunil [23]. Figure 3 (a,b,c,d, and e) shows the results of the Rietveld refinement process. Based on Fig. 3, it can be seen that there is a match between the measured data (+) and calculated data (red line). In addition to the visual agreement, this refinement process can be considered acceptable as it has a Goodness-of-Fit ( $\chi^2$ ) value below 4 [24]. The results of Rietveld refinement of the crystal structure of  $\text{TiO}_2$  films including lattice parameters,  $d$ -spacings, and the ratio of  $c/a$  compared with the results from A. Mustafa *et al.* [25] can be seen in Table 2. It can be seen that when the number of coatings increases, the lattice parameters increase with the reduction of the crystallite size indicating a quantum-size effect [26].

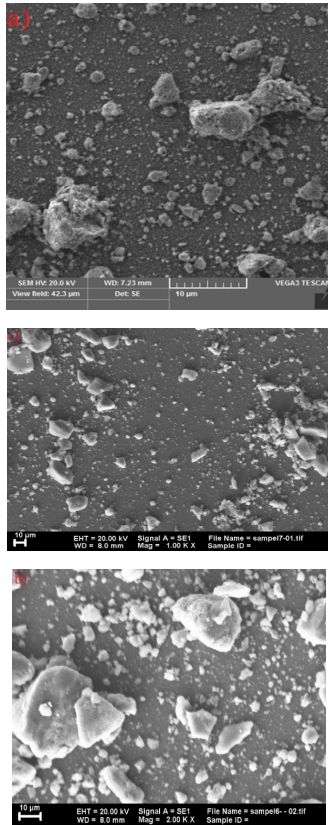


Fig. 4. Morphology of  $\text{TiO}_2$  films: a)  $\text{TiO}_2$  – 5 h, b)  $\text{TiO}_2$  – 10 h, and c)  $\text{TiO}_2$  – 25 h

## B. Morphology

Figure 4 shows the morphology of  $\text{TiO}_2$  film fabricated by the spin coating method. The  $\text{TiO}_2$  powder has a homogeneous shape, but many agglomerate particles are due to the low time duration and rotation velocity during the spinning process.

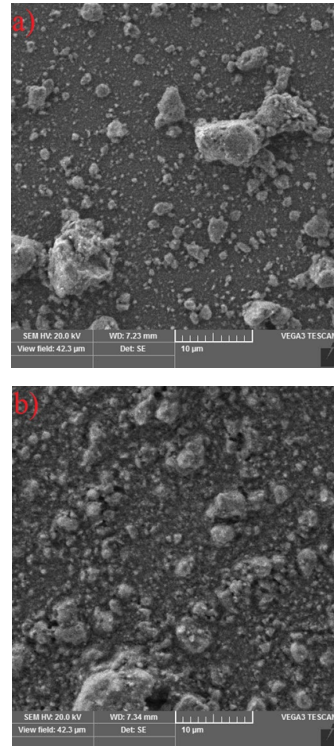


Fig. 5. Morphology of  $\text{TiO}_2$  films: a) 1x coating and b) 5x coatings

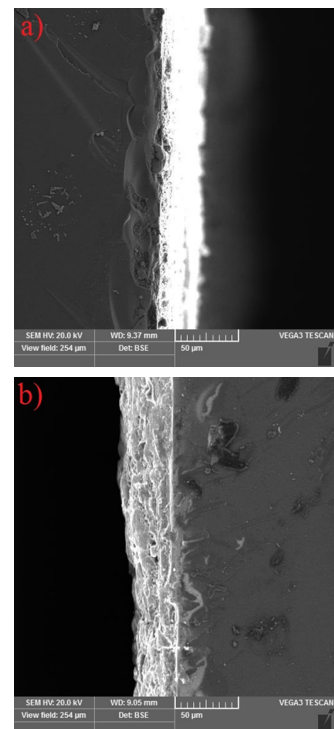


Fig. 6. Cross-section morphology of  $\text{TiO}_2$  films: a) 1x coating and b) 5x coatings

Figure 5 shows the morphology of the  $\text{TiO}_2$  – 5 h film as a variation of the number of coatings. Based on Fig. 5, the  $\text{TiO}_2$  – 5 h powder in the  $\text{TiO}_2$  film with five times of coating looks more compact and has many agglomerates due to the low homogeneity of the soluti-

on and high amount of the TiO<sub>2</sub> — 5 h powder in the substrate. Figure 6 shows the cross-section morphology of the TiO<sub>2</sub> — 5 h film at 1 and 5 times the number of coatings. Based on Fig. 6, the thickness of the film

was approximately 25 μm, which indicated that there is no difference in thickness. It was caused by TiO<sub>2</sub> — 5 h powder in the TiO<sub>2</sub> film with five times of coatings not enough to fill the substrate.

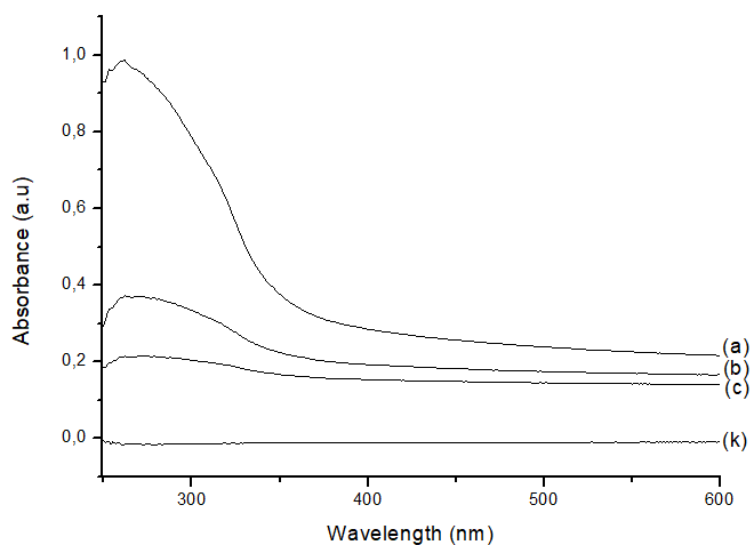


Fig. 7. UV-Vis absorption spectra of TiO<sub>2</sub> films: a) TiO<sub>2</sub> — 5 h, TiO<sub>2</sub> — 10 h, c) TiO<sub>2</sub> — 25 h, and k) glass substrate

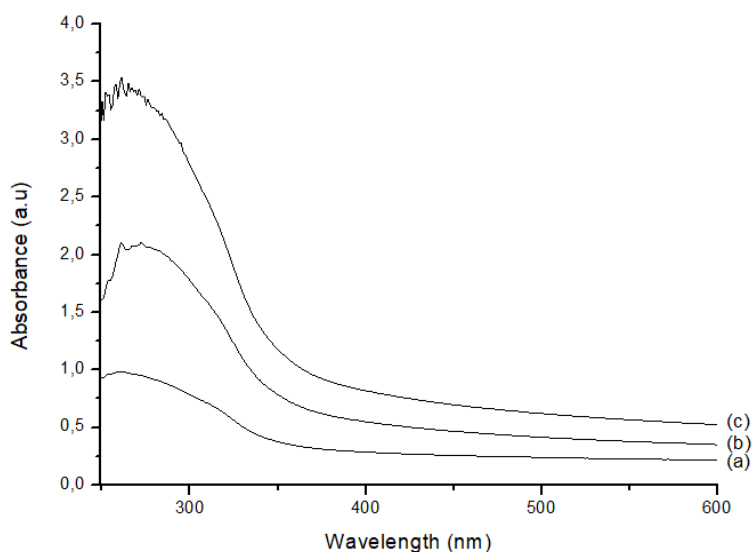


Fig. 8. UV-Vis absorption spectra of TiO<sub>2</sub> — 5 h films: a) 1x coating, b) 3x coatings, and c) 5x coatings

### C. UV-Visible characterization

Figures 7 and 8 show the absorption spectrum of the TiO<sub>2</sub> film as a variation of mixing duration and number of coatings, respectively. Based on these figures, it can be seen that the absorption range of the TiO<sub>2</sub> films is at a wavelength between 245 and 400 nm (UV spectrum). Also, the absorbance curve shifts to a long wavelength (lower energy) due to induced oxygen vacancies resulting in defects by aggregation [27]. Based on Fig. 8, the peak of absorbance shifts to lower energy or higher wavelength because of the increase in the number of coatings to 5 times due to the increase in particle size caused by agglomerate on the substrate surface. The agglomerate

of the TiO<sub>2</sub> particle on the substrate leads to a lower surface area [28] and creates a low grain boundary in the particle. Thus, lower energy is required to promote electrons from the valence band to the conduction band. The determination of the band gap energy of the TiO<sub>2</sub> film that has been fabricated can be estimated using the equation  $(\alpha h\nu)^{1/n} = A(h\nu - E_g)$  [29], where  $A$  is a constant value,  $E_g$  is the band gap energy of the TiO<sub>2</sub> film and  $n$  is a direct band gap transition with the value of  $n = 1/2$ . Further, the band gap can be estimated by plotting  $(\alpha h\nu)^{1/n}$  vs  $h\nu$  and the estimated band gap value was obtained from extrapolating the straight line of the graph on  $h\nu$  axis at the value of  $\alpha = 0$  [30] as shown in Fig. 9 (a,b,c,d and e).

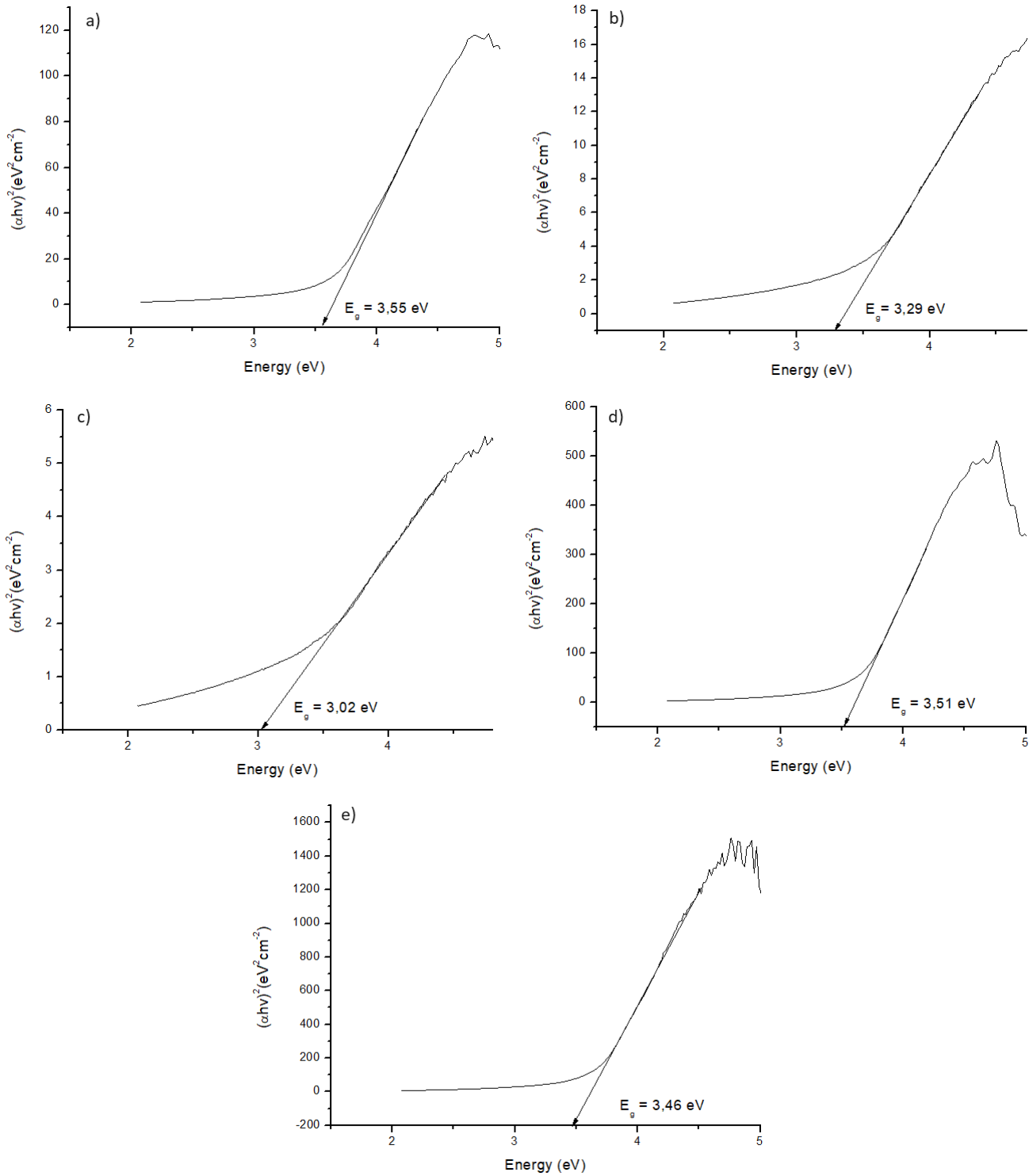


Fig. 9. Band gap energy of a) TiO<sub>2</sub> – 5 h, b) TiO<sub>2</sub> – 10 h, c) TiO<sub>2</sub> – 25 h, d) TiO<sub>2</sub> – 5 h (3x coatings), and e) TiO<sub>2</sub> – 5 h (5x coatings)

Based on the Fig. 9,a, the band gap energy of the TiO<sub>2</sub> – 5 h film is approximately 3.55 eV. The summary of energy gap values can be seen in Table 3. Based on Table 3, the band gap energy values of the TiO<sub>2</sub> films that have been fabricated are in the range of 3.02–3.55 eV. As a variation of the TiO<sub>2</sub> powder, the band gap energy decreases when the mixing duration increases. The band gap energy of TiO<sub>2</sub>

– 5 h has the highest band gap energy due to a decrease in the particle size. Decreasing particle size will give a higher surface area and more defects as a grain boundary. These defects make an electron need more energy to pass the grain boundary and shift the absorbance spectrum to a lower wavelength or a blue shift [20, 31]. Table 3 also shows that the band gap energy decreases as the number of coatings on the TiO<sub>2</sub> – 5 h

thickness layers increases. Decreasing band gap energy can be attributed to the increase in the particle size due to aggregation on the surface of the film that results in the low surface area [28] and the quantum size effect of the TiO<sub>2</sub> [32, 33].

Sample	Band gap energy (eV)
TiO <sub>2</sub> – 5 h	3.55
TiO <sub>2</sub> – 10 h	3.29
TiO <sub>2</sub> – 25 h	3.02
TiO <sub>2</sub> – 5 h (3x coatings)	3.51
TiO <sub>2</sub> – 5 h (5x coatings)	3.46

Table 3. Band gap energy value of TiO<sub>2</sub> films fabricated by the spin coating method

Consequently, low energy is required for electrons to cross the grain boundary. Another reason can be correlated with the crystallinity of the sample. Sample TiO<sub>2</sub> – 5 h with five times of coatings has the highest crystallinity, resulting in the lowest surface defect. Thus, an electron needs low energy to excite from the valence band to the conduction band of the TiO<sub>2</sub> film [34].

#### D. Photocatalytic activity

The degradation of methylene blue 12 mg/l solution after 5 hours of irradiation with a UV lamp in a UV chamber was used to assess the activity of the TiO<sub>2</sub> film photocatalyst. Figure 10 shows the photocatalytic activity of the TiO<sub>2</sub> film as a variation of the TiO<sub>2</sub> powder.

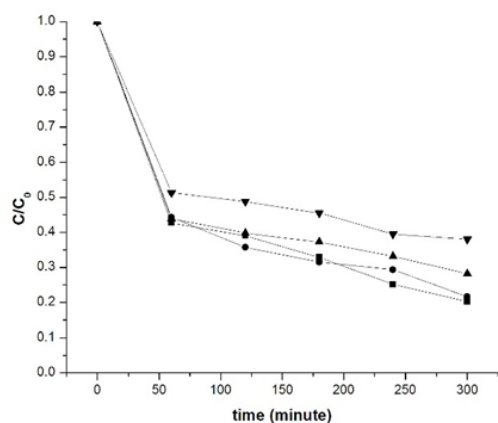


Fig. 10. The photodiscoloration of methylene blue over TiO<sub>2</sub> films as a function of UV light irradiation time (■ = TiO<sub>2</sub> – 5 h, ● = TiO<sub>2</sub> – 10 h, ▲ = TiO<sub>2</sub> – 25 h, and ▼ = commercially available TiO<sub>2</sub>)

Based on Fig. 10, the TiO<sub>2</sub> – 5 h film gives the best photocatalytic activity compared with other samples. The TiO<sub>2</sub> – 5 h film has the most significant amount of catalyst TiO<sub>2</sub> on the substrate (about 1.2 mg). Increasing the amount of catalyst TiO<sub>2</sub> in methylene blue solution will increase the amount of superoxide ion (O<sup>2-</sup>) and hydroxyl radicals (OH) that give good photocatalytic activity on the TiO<sub>2</sub> – 5 h film. Among the TiO<sub>2</sub> – 10 h and TiO<sub>2</sub> – 25 h films with the same amount

of catalyst TiO<sub>2</sub> on their surface, the TiO<sub>2</sub> – 10 h gives a better catalytic activity performance than that of TiO<sub>2</sub> – 25 h. Even though the samples have the same amount of catalyst (0.5 mg), they are different in crystallite size, and the crystallite size of TiO<sub>2</sub> – 25 h was 5.94 nm lower than TiO<sub>2</sub> – 10 h (7.66 nm). The crystallite size is critical in photocatalytic activity. When the crystallite size reduces below approximately 10 nm, grain boundaries dominate the material and act as trap sites for photogenerated charge carriers, enhancing their recombination probability [34, 35]. The value of photocatalytic degradation,  $k$ , can be determined using the Langmuir–Hinshelwood method by plotting  $\ln(C_0/C)$  vs time [31] in Fig. 11. Based on Fig. 11, the TiO<sub>2</sub> – 5 h film has the most excellent value of  $k$  ( $k = 0.0032/\text{min}$ ) than compared to other samples (TiO<sub>2</sub> – 10 h = 0.0027/min, TiO<sub>2</sub> – 25 h = 0.0018/min and commercially available TiO<sub>2</sub> = 0.0014/min).

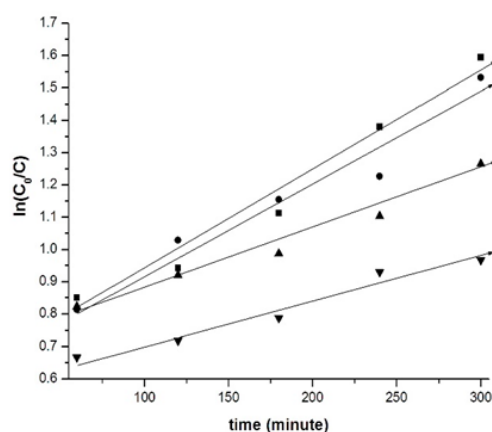


Fig. 11. Kinetic linear fitting curves of MB dye over TiO<sub>2</sub> films under UV irradiation (■ = TiO<sub>2</sub> – 5 h, ● = TiO<sub>2</sub> – 10 h, ▲ = TiO<sub>2</sub> – 25 h, and ▼ = commercially available TiO<sub>2</sub>)

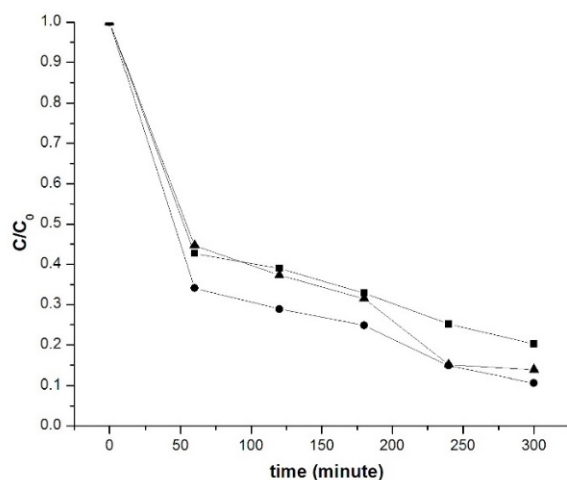


Fig. 12. The photodiscoloration of MB dye over TiO<sub>2</sub> – 5 h films under UV light irradiation (■ = 1x coating, ● = 3x coatings, and ▲ = 5x coatings)

Figure 12 shows the photocatalytic activity of the  $\text{TiO}_2$  — 5 h film as a variation of the number of coatings. Based on Fig. 12, sample  $\text{TiO}_2$  — 5 h with three times of coating has the best photocatalytic activity in methylene blue solution due to an increase in the amount of  $\text{TiO}_2$  catalyst on the substrate that increases the number of active sites on the catalyst surface and increases the catalytic activity [34]. When the coating increases to 5 times, there is a decrease in photocatalytic activity in  $\text{TiO}_2$  — 5 h film with five times of coatings.

Generally, the number of active sites on the catalyst's surface increases as its mass increases. When the amount of catalyst  $\text{TiO}_2$  on the substrate surface is higher than the minimum value, an agglomerate of particles will be created. It will decrease the efficiency of photocatalytic activity because the UV light is not absorbed fully by the catalyst, resulting in fewer electron-hole pairs [36]. Conversely,  $\text{TiO}_2$  in the nether part of the films makes it hard to contact the reactant, and reaction products make it difficult to enter the solution. Also, the aggregation of

$\text{TiO}_2$  particles causes a decrease in the number of active surface sites [30] and prevents the degradation process, decreasing the oxidation rate [37]. Andronic et al. noticed a similar result: when all dye molecules are absorbed on  $\text{TiO}_2$ , adding more  $\text{TiO}_2$  has no effect on the degradation efficiency, and it may cause an increased opacity of the suspension due to the excess of  $\text{TiO}_2$  particles [38].

#### IV. CONCLUSION

The  $\text{TiO}_2$  films having anatase phase were successfully fabricated by spin coating method from nanopowders prepared by co-precipitation method by varying the mixing duration and the number of coatings. The band gap of the resulting  $\text{TiO}_2$  films is in the range of 3.02 — 3.55 eV. Analysis of photocatalytic activity by degradation of methylene blue solution shows that sample  $\text{TiO}_2$  — 5 h and  $\text{TiO}_2$  — 5 h with three times of coatings have the best photocatalytic activity.

- 
- [1] J. Ovenstone, K. Yanagisawa, *Chem. Mater.* **11**, 66 (2021); <https://doi.org/10.1021/cm990172z>.
- [2] A. Castro, M. Nunes, A. Carvalho, F. Costa, M. Florencio, *Solid State Sci.* **10**, 602 (2008); <https://doi.org/10.1016/j.solidstatesciences.2007.10.012>.
- [3] P. Nyamukamba, O. Okoh, H. Mungondori, R. Taziwa, S. Zinya, in *Titanium Dioxide*, edited by D. Yang (IntechOpen, Rijeka, 2018), Chap. 8; <https://doi.org/10.5772/intechopen.75425>.
- [4] R. Vijayalakshmi, V. Rajendran, *Arch. App. Sci. Res.* **4**, 1183 (2012).
- [5] A. K. Tripathi *et al.*, *Mat. Sci. Sem. Proc.* **23**, 136 (2014); <https://doi.org/10.1016/j.mssp.2014.02.041>.
- [6] B. R. Fernandez, *Makalah. Sintesis Nanopartikel* (Pasca sarjana Universitas Andalas, Padang, 2011).
- [7] H. N. Widaryanti, Darminto, *AIP Conf. Proc.* **1555**, 11 (2013); <https://doi.org/10.1063/1.4820981>.
- [8] V. Zharvan, G. Yudoyono, D. Darminto, *J. Fis. Apl.* **19**, 25 (2023); <https://doi.org/10.12962/j24604682.v19i1.15475>.
- [9] A. J. Haider, Z. N. Jameel, I. H. Al-Hussaini, *Energy Procedia* **157**, 17 (2019); <https://doi.org/10.1016/j.egypro.2018.11.159>.
- [10] A. A. Daniyan *et al.*, *J. Minerals Mater. Charact. Eng.* **2**, 15 (2014); <https://doi.org/10.4236/jmmce.2014.21003>.
- [11] V. T. Lukong, K. Ukoba, T.-C. Jen, *Int. J. Adv. Manuf. Tech.* **122**, 3525 (2022); <https://doi.org/10.1007/s00170-022-10043-3>.
- [12] A. Hosseini, K. Ç. İçli, M. Özenbaş, Ç. Erçelesi, *Energy Procedia* **60**, 191 (2014); <https://doi.org/10.1016/j.egypro.2014.12.332>.
- [13] T. Senthil, N. Muthukumarasamy, S. Agilan, M. Thambidurai, R. Balasundaraprabhu, *Mater. Sci. Eng. B* **174**, 102 (2010); <https://doi.org/10.1016/j.mseb.2010.04.009>.
- [14] A. Elfanaoui *et al.*, *Int. J. Hydrog. Energy* **36**, 4130 (2011); <https://doi.org/10.1016/j.ijhydene.2010.07.057>.
- [15] S. Amole *et al.*, *J. Mater. Sci. Chem. Eng.* **7**, 23 (2019); <https://doi.org/10.4236/msce.2019.76003>.
- [16] R. Mori *et al.*, *J. Mater. Sci.* **46**, 1341 (2011); <https://doi.org/10.1007/s10853-010-4925-2.9>.
- [17] C. F. Holder, R. E. Schaak, *ACS Nano* **13**, 7359 (2019); <https://doi.org/10.1021/acsnano.9b05157>.
- [18] Y. Zhao *et al.*, *Mater. Lett.* **61**, 79 (2007); <https://doi.org/10.1016/j.matlet.2006.04.010>.
- [19] C. Euvananont, C. Junin, K. Inpor, P. Limthongkul, C. Thanachayanont, *Ceram. Int.* **34**, 1067 (2008); <https://doi.org/10.1016/j.ceramint.2007.09.043>.
- [20] L. Ge, M. Xu, M. Sun, H. Fang, *J. Sol-Gel Sci. Technol.* **38**, 47 (2006); <https://doi.org/10.1007/s10971-006-6009-y>.
- [21] S. Yang, Y. Liu, Y. Zhang, D. Mo, *Bull. Mater. Sci.* **33**, 209 (2010); <https://doi.org/10.1007/s12034-010-0032-x>.
- [22] P. Gluchowski *et al.*, *J. Phys. Chem. C* **126**, 7127 (2022); <https://doi.org/10.1021/acs.jpcc.2c00672>.
- [23] S. Rohilla, *IOP Conf. Ser.: Mater. Sci. Eng.* **872**, 012171 (2020); <https://doi.org/10.1088/1757-899X/872/1/012171>.
- [24] E. H. Kisi, *Mater. Forum* **18**, 135 (1994).
- [25] A. Mustafa *et al.*, *Surf. Eng.* **37**, 784 (2021); <https://doi.org/10.1080/02670844.2020.1813517>.
- [26] G. Li, J. Boerio-Goates, B. F. Woodfield, L. Li, *App. Phys. Lett.* **85**, 2059 (2004); <https://doi.org/10.1063/1.1790596>.
- [27] M. F. Sidra Jamil, *Mater. Innov.* **1**, 21 (2021); <https://doi.org/10.54738/MI.2021.1103>.
- [28] I. Gosens *et al.*, *Part. Fibre Toxicol.* **7**, 1 (2010); <https://doi.org/10.1186/1743-8977-7-37>.
- [29] N. Das, P. Ghosh, M. Mitra, K. Chattopadhyay, *Physica E* **42**, 2097 (2010); <https://doi.org/10.1016/j.phys.e.2010.03.035>.
- [30] S. Kale *et al.*, *Appl. Surf. Sci.* **253**, 4335 (2007); <https://doi.org/10.1016/j.apsusc.2006.09.043>.
- [31] H. Zhang *et al.*, in *The 7th National Conference on Functional Materials and Applications* (Changsha,



- Hunan, China, 2010), p. 359.
- [32] B. Avinash *et al.*, AIP Conf. Proc. **1728**, 020426 (2016); <https://doi.org/10.1063/1.4946477>.
- [33] M. El-Hagary, E. Shaaban, S. Moustafa, G. Gad, Solid State Sci. **91**, 15 (2019); <https://doi.org/10.1016/j.solidstatesciences.2019.03.005>.
- [34] K. Eufinger, D. Poelman, H. Poelman, R. De Gryse, G. Marin, in *Thin Solid Films: Process and Applications*, edited by S. C. Nam (Transworld Research Network, India, 2009), p. 189.
- [35] O. Carp, C. Huisman, A. Reller, Prog. Solid State Chem. **32**, 33 (2004); <https://doi.org/10.1016/j.progsolidstchem.2004.08.001>.
- [36] J. Yu, X. Zhao, Q. Zhao, J. Mater. Sci. Lett. **19**, 1015 (2000); <https://doi.org/10.1023/A:1006705316651>.
- [37] J. Santhanalakshmi, R. Komalavalli, P. Venkatesan, J. Nanosci. Nanotechnol. **2**, 8 (2012); <https://doi.org/10.5923/j.nm.20120201.02>.
- [38] L. Andronic, A. Duta, Mater. Chem. Phys. **112**, 1078 (2008); <https://doi.org/10.1016/j.matchemphys.2008.06.059>.

## ОПТИЧНО АКТИВНІ ПЛІВКИ TiO<sub>2</sub>, ВИГОТОВЛЕНІ МЕТОДОМ ЦЕНТРИФУГУВАННЯ ДЛЯ ФОТОРЕМЕДІАЦІЇ МЕТИЛЕНОВОГО СИНЬОГО

Вікран Зарван<sup>1</sup>, Гатут Юдойоно<sup>2</sup>, Дармінто<sup>2</sup>

<sup>1</sup> Університет Негері Макаassar, Індонезія,

e-mail: vicran.zarvan@unm.ac.id

<sup>2</sup> Інститут технологій Сепулук Нопембер, Індонезія

Для успішного створення шару TiO<sub>2</sub> використовували центрифугування. Плівка TiO<sub>2</sub> була створена розчиненням нанопорошку TiO<sub>2</sub> у терпінеолі та етилцелюлозі, а потім нанесенням його на скло Coating. Згодом форму, фазу та оптичні властивості плівок визначали за допомогою сканувальної електронної мікроскопії, X-променевої дифракції та УФ-спектроскопії. Фотокаталітичні вимірювання плівок TiO<sub>2</sub> проводили за допомогою УФ-лампи з опроміненням розчину метиленового синього 12 мг/л протягом 5 годин. Відповідно до результатів усі плівки TiO<sub>2</sub> мають анатазну фазу зі значеннями розміру кристалітів у діапазоні від 5.55 нм до 6.94 нм і ділянкою поглинання поблизу ультрафіолетового діапазону. Найкращу фотокаталітичну активність виявили в плівки, що містить частинки TiO<sub>2</sub>, яку перемішували протягом 5 годин зі значенням сталої швидкості знебарвлення барвника 0.0032/хв.

**Ключові слова:** TiO<sub>2</sub>, анатаз, тонкоплівковий, фотокаталізатор.